光学学报

# 基于CGH多镜定姿定态的离轴光学系统装调方法

吴一凡[1,2]，陈建发[1,2*]，崔泽曜[1,2]，黄浩阳[1,2]
[1]中国航空工业集团公司洛阳电光设备研究所，河南 洛阳 471009；
[2]空基信息感知与融合全国重点实验室，河南 洛阳 471009

**摘要** 针对离轴光学系统装调过程中自由度高且互相耦合的问题，提出一种新的离轴自由曲面反射式光学系统装调方法，采用计算全息图(CGH)实现多镜共基准定姿定态，解耦合系统各镜片的装调自由度，显著降低系统装调复杂度；分析CGH用于定姿定态时的定位精度，提高系统装调精度和效率，适应不同构型的离轴光学系统。利用上述方法，完成口径为210 mm、视场为2°×2°的近红外长波红外双波段离轴反射式光学系统装调，全视场波像差RMS小于0.126$\lambda$($\lambda$=632.8 nm)，达到设计预期，装配周期短，成像质量优良。

**关键词** 光学设计；计算全息图；离轴三反；自由曲面
**中图分类号** O438；O436；O439 **文献标志码** A **DOI**：10.3788/AOS231547

## 1 引 言

机载光电系统多功能、高性能、轻量化的发展趋势，对光学系统研制提出了更高的要求。反射式光学系统因其宽波段、紧凑化的工作特性被广泛应用到各类机载光电设备中，其中自由曲面离轴三反光学系统能够弥补传统同轴反射系统次镜遮拦、视场小及优化自由度低的缺点。随着自由曲面设计加工技术的发展和成熟，自由曲面面形检测和系统装调成为当前限制自由曲面离轴反射式系统应用的关键[1-2]。

2013年，中国科学院长春光机所王超等[3-4]利用双计算全息图(CGH)分别对次镜、三镜定位，研制了一套三镜消像散系统。以三镜面形检测CGH为基准开展系统装调，实现了0.16$\lambda$(全文若无特殊说明，$\lambda$=632.8 nm)全视场波像差RMS。该方法采用双CGH进行基准传递，存在误差积累。同年，中国科学院西安光机所庞志海[5]使用逆向优化法对自由曲面离轴三反光学系统进行全过程计算机辅助装调，实现了0.09$\lambda$的全视场波像差RMS。但是全过程计算机辅助逆向优化法的鲁棒性较差，难以支持大误差系统的研制，且计算过程中会出现非唯一解，导致装调周期难以控制。2020年，中国科学院长春光机所李蕾[6]针对自由曲面离轴三反系统的失调量敏感度矩阵开展研究，建立离轴三反系统失调量求解模型，使用该模型指导装调能够有效降低系统平均波像差，经过两轮迭代后平均波像差RMS从0.6$\lambda$降低到0.1$\lambda$以下。

目前，关于自由曲面离轴反射系统装调方法的研究聚焦在基准精度提高和计算机辅助装调模型设计，但离轴系统装调自由度多、复杂度较高，因此上述方法存在误差的传递难以抑制，导致装调周期长、效果不佳。本文提出一种基于CGH的多镜定姿定态装调方法，实现了多镜片装调自由度解耦合，从而控制误差传递，降低系统装调复杂度。利用该方法可在短周期内完成一套自由曲面离轴三反系统装调，成像质量中心的视场波像差RMS为0.079$\lambda$。

## 2 装调理论及方法

在以往的研究中，CGH用于单镜面形检测的技术较为成熟，但对多镜片面形检测区域进行共基准设计，并将待测面空间位置作为参数参与多镜定姿定态CGH设计，国内尚未有公开报道。本文提出一种基于多镜面形检测CGH共基准设计实现装调时各镜面独立高精度定位的装调方法，其设计思路的核心在于：1)检测与设计联合，保证系统实现面形高精度检测，同时实现多镜片高精度定姿定态；2)多自由度解耦，大幅降低装调复杂度，提升装调效率和精度。

### 2.1 共基准面形检测与定姿定态联合CGH设计

与单镜检测CGH不同，为实现多镜共基准定姿定态装配设计，需要添加镜片离轴量、镜片姿态倾角等额外参数信息，以满足兼顾镜面CGH检测与实现多镜间多参数计算机辅助装调、基准传递、镜片定姿定位的设计要求。CGH设计流程如图1所示。在CGH设计过程中，为满足共基准设计需求，需反复迭代优化，视情

**收稿日期**：2023-09-13；**修回日期**：2023-09-28；**录用日期**：2023-10-10；**网络首发日期**：2023-11-14
**通信作者**：*biterika@qq.com

况调整CGH设计参数,直至同时满足双镜定姿定态且可加工的CGH设计要求。具体设计过程如下:

1)输入所设定的待测面参数,包括姿态参数和面形参数。

2)根据参数计算CGH姿态优化初始点。优化CGH姿态参数(CGH倾斜量、CGH相对待测面距离),使主镜、三镜面形检测全息区域完整,且大小适中,便于检测。

3)根据姿态参数设计其余辅助全息区域,包括粗对准全息区域、角度对准全息区域、干涉级次标记全息区域。其中,角度对准全息区域采用反射光栅设计,闪耀角度为所设计的干涉仪光线入射角度。入射角度由干涉条纹对比度公式确定,即

$$\gamma=\frac{2\sqrt{C}}{1+C}\ (\gamma>0.3),\ C=\frac{I_{\text{test}}}{I_{\text{ref}}},\tag{1}$$

式中:$I_{\text{test}}$和$I_{\text{ref}}$分别表示测试光强与参考光强;$\gamma$表示条纹清晰度。调整衍射效率以适配参考光与待测光光强比约为1:0.04。

4)考察设计条纹的可加工性[7],若条纹满足加工要求,则认为完成定姿定态CGH设计,可以进行系统装调;否则返回步骤1),重新调整设计参数直至条纹满足加工要求。

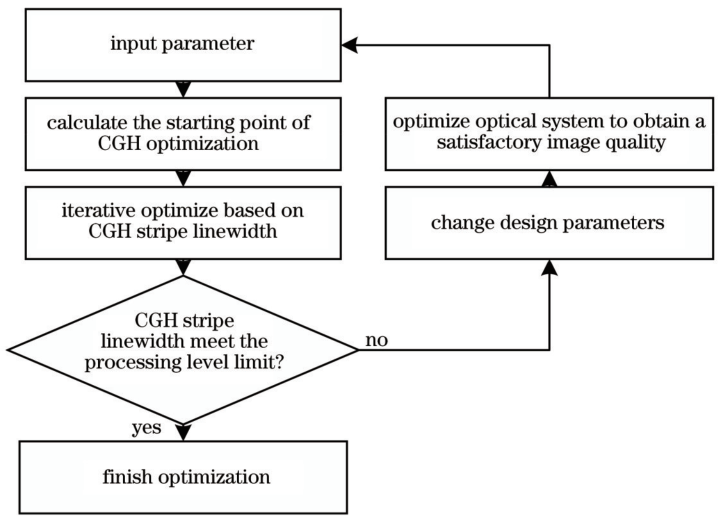


图1　CGH设计流程

Fig. 1　CGH design flow

单次CGH设计流程中可能出现无法满足加工要求的情况,因此在设计过程中设置反馈环节,以保证光学系统的检测性与装配性。在反馈环节中对设计提出改进要求以适应装调方法,改变曲率半径或调整镜片间相对姿态。图2显示,光学系统设计优化过程中,元件曲率半径、元件尺寸变化与对应CGH线宽呈线性关系,待测面曲率半径越大,对应CGH条纹越宽,而全部待测面的最小包络圆半径越小,对应CGH条纹越宽。

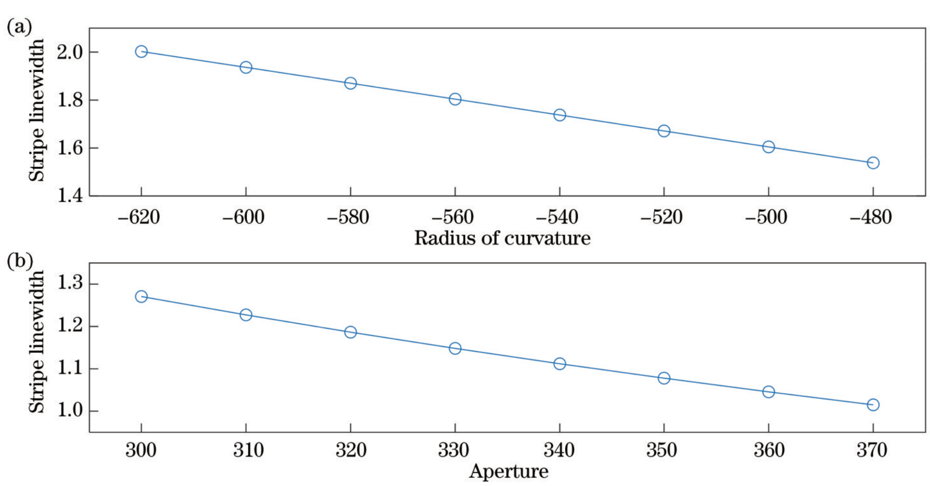


图2　CGH条纹线宽变化趋势。(a)镜面曲率半径影响;(b)全镜片包络口径影响

Fig. 2　Trends in stripe linewidth of CGH. (a) Effect of raidus of curvature; (b) effect of envelope aperture

### 2.2 基于多参数计算机辅助装调与CGH共基准传递装调的方法

离轴系统的单镜片有6个自由度，传统装调方法中镜片存在耦合，过高的复杂度导致系统装调困难，目前常用的降低系统装调难度的方法为基准传递方法[8-10]和共基准设计方法[11]。本研究采用共基准设计的CGH实现主镜、三镜的定姿定态，提高装调定位精度，实现各镜片解耦合，避免误差在传递中扩大，同时避免系统调节过程陷入局部最优解。装调方法的流程如图3所示，具体细节如下：

1）根据设计的系统参数完成双镜定姿定态CGH设计；

2）设置CGH装调基准，以CGH主镜对准区域为装调基准，调整干涉仪与CGH主镜对准区对准并固定；

3）主镜装调，根据主镜干涉仪对准全息区域调整干涉仪姿态，姿态定位失调量由该检测光路的灵敏度矩阵反映，根据灵敏度矩阵理论，小失调量时Zernike多项式系数与失调量呈线性关系[12-15]，此时根据干涉条纹Zernike系数精调主镜；

4）三镜装调，根据三镜干涉仪对准全息区域调整干涉仪姿态，并根据干涉条纹Zernike系数精调三镜，完成主镜、三镜定姿定态；

5）建立系统装调基准，以干涉仪为基准，使用经纬仪对准系统基准和出瞳处准直镜至轴上零视场；

6）次镜装调，使用准直激光定位次镜姿态滚转和倾斜；

7）精调次镜，使系统零视场成像质量达到设计要求；

8）调整干涉仪和准直镜到轴外视场的角度，测量轴外视场成像质量，若满足设计要求，结束系统装调，否则回到零视场继续调整波像差，直到轴外视场也满足设计要求。

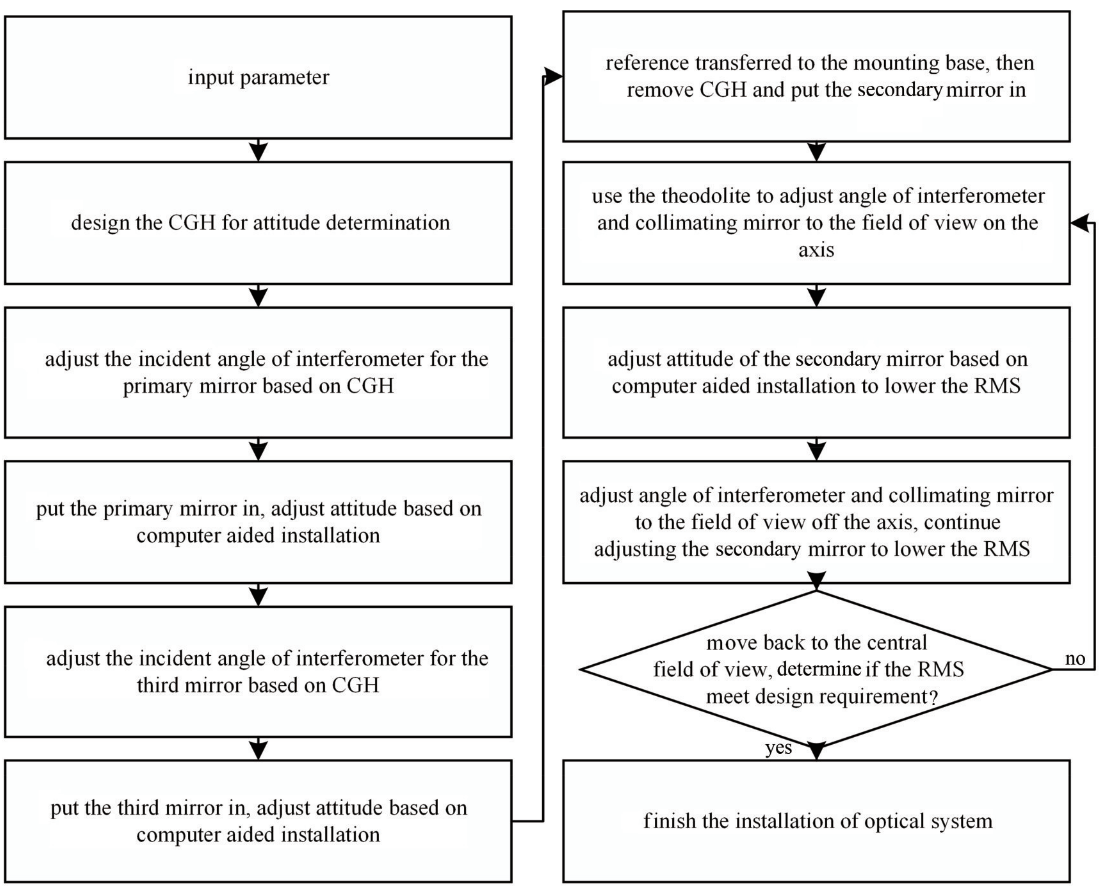


图3 装调方法流程图

Fig. 3 Adjustment flow diagram

## 3 仿真设计与误差分析

### 3.1 设计参数

光学系统设计参数如表1所示，自由曲面离轴三反系统的光路如图4所示。CGH条纹的加工极限为1.5 μm，口径限制单全息区域不超过80 mm，完整CGH口径不超过160 mm。

### 3.2 CGH光路布局设计

依据2.2节给出的设计流程完成图5(a)所示的CGH设计，条纹最小线宽为1.78 μm，两个主全息区域的口径分别为75 mm和60 mm，完整口径为150 mm，满足制造工艺和设计要求。在光学成像设计软件CODEV中进行面形检测的仿真，共基准CGH测试光路如图5(b)所示。

表1　系统设计参数

Table 1　Designed system parameters

| Parameter | Value |
| --- | --- |
| Light aperture of primary mirror | 210 mm |
| Light aperture of third mirror | 120 mm |
| Operating band | Near infrared(NIR) band: 0.7–0.9 μm; Long wave infrared(LWIR) band: 8–12 μm |
| Field of view(FoV) | NIR band: 0.4°×0.4°; LWIR band: 2°×2° |
| Imaging quality | Full FoV of NIR RMS: <0.10λ; Full FoV of LWIR RMS: <0.23λ |

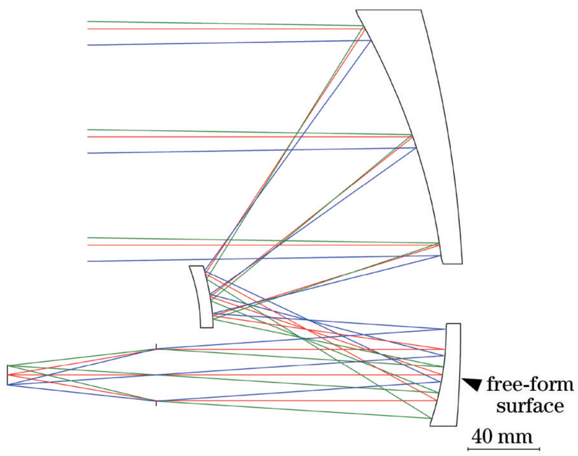


图4　离轴三反系统光路图

Fig. 4　Drawing of the lighpath of off-axis TMA system

### 3.3　共基准传递CGH误差分析

共基准传递CGH定位精度受设计误差与制备误差影响。基于系统设计主镜、三镜面形参数和空间位置参数生成仿真模型，CGH模型使用3.2节的设计结果，仿真结果为设计的CGH波前与实际待测面的面形误差。误差表示设计的CGH透射波前与实际待测面的面形误差，误差仿真结果如图6所示，主镜检测面形RMS为0.017λ，三镜检测面形RMS为0.016λ。

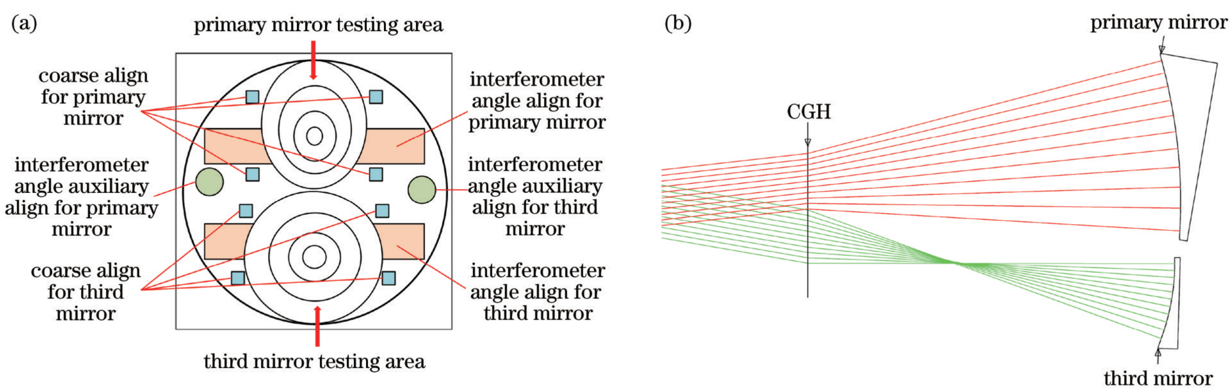


图5　CGH设计。(a)CGH设计图；(b)共基准CGH测试光路图

Fig. 5　Drawing of CGH design. (a) Drawing of CGH design; (b) drawing of the lighpath for two mirrors locating

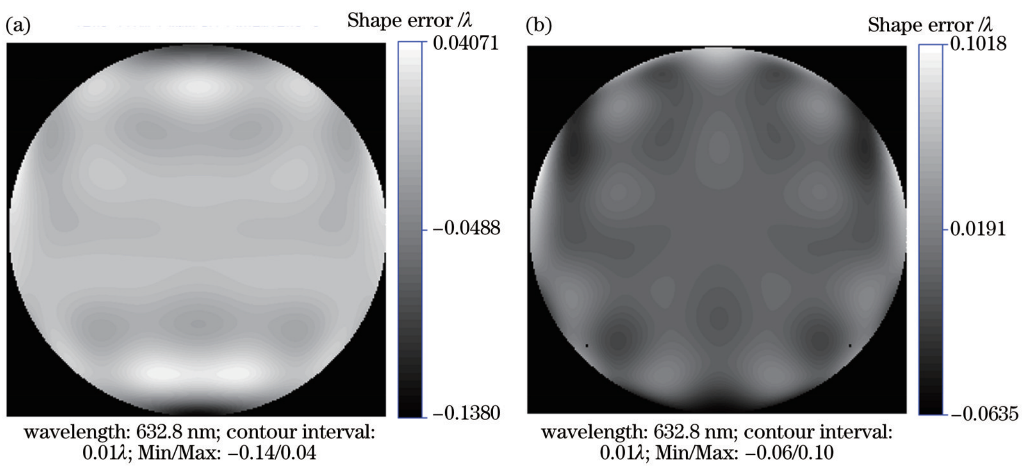


图6　主镜和三镜CGH面形检测仿真结果。(a)主镜检测仿真结果；(b)三镜检测仿真结果

Fig. 6　Simulation results of CGH shape detection for primary mirror and third mirror. (a) Result of primary mirror; (b) result of third mirror

制备误差分析可以简化所提模型为线性光栅模型[12,16-17]，如图 7 所示。其中，$S$ 为光栅周期，$b$ 为蚀刻区域线宽，占空比 $D=b/S$，$A_0$ 和 $A_1$ 分别为未蚀刻区域与蚀刻区域透射波前振幅，在相位型CGH中二者的差可忽略不计，$\phi$ 为未蚀刻区域与蚀刻区域的相位深度差。

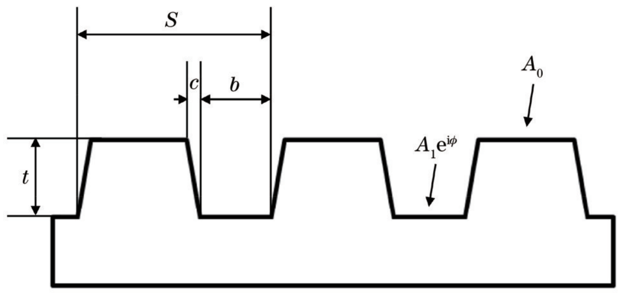


图 7　简化CGH光栅模型

Fig. 7　Simplified CGH model

主要制备误差为基底面形误差、条纹线宽误差、蚀刻深度误差和条纹占空比误差。其中对CGH成像影响最大的是基底面形误差，但基板的制作精度小于 $\lambda/100$，且不影响后续刻蚀条纹的制备，因此不予关注。计算得到的其余主要制造误差数值如表 2 所示。其余误差在公差范围内引起的波像差变化均小于 $\lambda/90$，对CGH定位精度的影响微小。生产制造中应首先抑制基板面形误差，其次关注条纹线宽误差，以进一步提高CGH面形检测精度。

表 2　CGH制造中主要误差对波前的影响

Table 2　Influence on wavefront by primary error in CGH fabrication

| Type | Tolerance | RMS /λ |
|---|---|---|
| Stripe linewidth | 0.2 μm | 0.011 |
| Etching depth | 1% | 0.005 |
| Duty cycle | 1% | — |

### 3.4　CGH定位精度与系统公差分析

对实际加工的CGH成品进行透射波前检测，结果如图 8 所示。由图 8 可知，主镜全息区域 0 级透射波前误差为 7.8 nm，面形检测时带来误差约 0.0123$\lambda$，而三镜全息区域 0 级透射波前误差为 6.7 nm，面形检测时带来误差约 0.0106$\lambda$，符合设计预期，满足定姿定态精度要求。

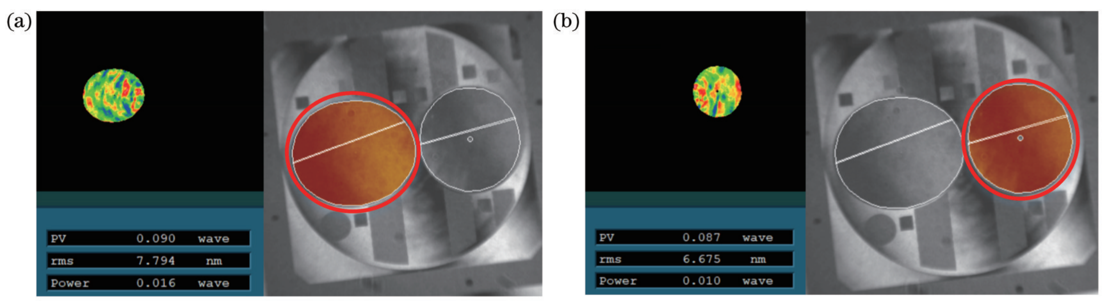


图 8　CGH透射波前检测结果。(a)主镜全息区域检测结果；(b)三镜全息区域检测结果

Fig. 8　Results of transmitted wavefront of CGH. (a) Result of primary mirror holographic region; (b) result of third mirror holographic region

CGH实测误差数据如表 3 所示，其中透射波前误差为平行光入射全息区域的 0 级透射波前误差，综合波前误差小于 $\lambda/80$，达到面形检测精度要求。

通过干涉仪测试结果计算CGH定位精度。实际干涉仪测量时 Zernike 系数计算到小数点后两位，根据 Zernike 系数精度 0.01，分别计算得到主镜和三镜的各参数定位精度如表 4 所示。主镜沿 $Y$ 方向的离轴量为 35.0 μm，离焦量($Z$)为 2.1 μm，俯仰角($\alpha$)为 13.68″，方位角($\beta$)为 10.08″，滚转角($\gamma$)为 92.16″；三镜沿 $Y$ 方向的离轴量为 65.8 μm，离焦量为 3.0 μm，俯仰角为 12.24″，方位角为 26.64″，滚转角为 483.80″。

表 3　实物CGH误差分析

Table 3　Error of physical CGH

| Type | Error | RMS /λ |
|---|---|---|
| Primary area RMS | 7.8 nm | 0.0123 |
| Third area RMS | 6.7 nm | 0.0106 |
| Duty cycle | 0.4% | 0.0032 |

光学系统公差分析首先依据加工装调经验生成一组公差限，进行蒙特卡罗模拟统计，选择放松或收紧公差限，最终得到一个合理的公差范围。高斯概率密度

表 4　CGH定位精度

Table 4　CGH locating accuracy

| Mirror | α /(″) | β /(″) | γ /(″) | X decenter /μm | Y decenter /μm | Z /μm |
|---|---|---|---|---|---|---|
| Primary mirror | 13.68 | 10.08 | 92.16 | 26.1 | 35.0 | 2.1 |
| Third mirror | 12.24 | 26.64 | 483.80 | 51.9 | 65.8 | 3.0 |

函数公差分布以及蒙特卡罗统计1000次的公差分析结果所给出的公差极限如表5所示，其中补偿量来自次镜，可满足90%概率下系统中心视场波像差RMS优于0.08λ。对比CGH定位精度与系统公差范围，各项参数定位精度均满足系统公差要求，因此认为该定位精度下装调系统可满足设计要求。

表5 各类公差限范围

Table 5 Value range of various tolerances

| Tolerance type | Primary mirror | Third mirror |
|---|---|---|
| *X* decenter /μm | ±50 | ±100 |
| *Y* decenter /μm | ±50 | ±100 |
| *Z* /μm | ±5 | ±5 |
| Tilt /(″) | ±100 | ±500 |

## 4 基于CGH双镜定姿定态装调方法验证

基于共基准CGH多镜定姿定态的装配光路如图9所示。首先装调主镜，单镜面形RMS为0.022λ；然后装调三镜，单镜面形RMS为0.032λ，达到单镜装调面形RMS小于0.050λ的设计要求；最后装调次镜，最终测量中心视场波像差RMS为0.079λ，如图10所示。

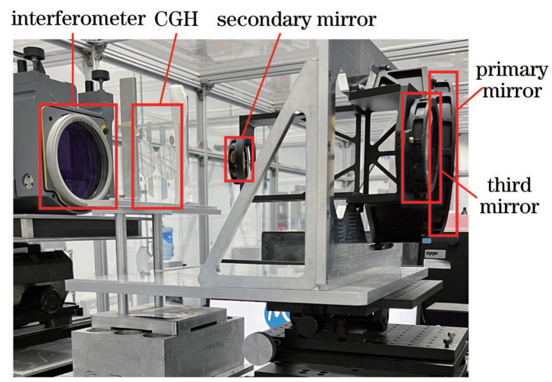


图9 基于共基准CGH多镜定姿定态装配光路图

Fig. 9 Lightpath of optical system attitude determination using CGH

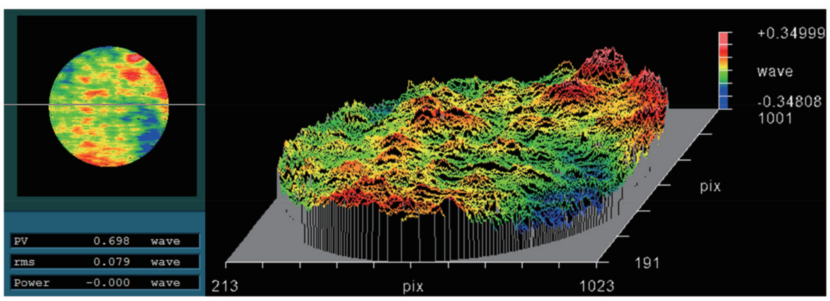


图10 系统中心视场测试结果

Fig. 10 Result of wavefront error measurement of center field of view

全视场成像质量特征点数据如表6所示。视场角调节通过经纬仪定位，并旋转光学系统实现。从表6可以看到，近红外光波段全视场波像差RMS小于0.093λ，长波红外波段全视场波像差RMS小于0.126λ，中心视场波像差RMS为0.079λ，达到设计对成像质量的要求。

表6 全视场波前误差测试结果

Table 6 Results of wavefront error measurement of full field of view

| Elevation angle $\alpha$ /(°) | WFE RMS of full FoV/λ | | | | |
|---|---|---|---|---|---|
| | $\beta$=−1° | $\beta$=−0.2° | $\beta$=0° | $\beta$=0.2° | $\beta$=1° |
| −1 | 0.126 | — | 0.118 | — | 0.089 |
| −0.2 | — | 0.083 | 0.084 | 0.080 | — |
| 0 | 0.096 | 0.093 | 0.079 | 0.085 | 0.078 |
| 0.2 | — | 0.087 | 0.088 | 0.082 | — |
| 1 | 0.084 | — | 0.113 | — | 0.080 |

## 5 结　论

提出一种基于CGH的多镜同步定姿定态装调方法，实现自由曲面离轴反射式光学系统镜片间的解耦合，显著降低系统装调难度，缩短装调周期，提高装调效率和精度。同时给出装调对设计的要求，通过指导设计迭代提高方法的适用性。基于CGH的定位精度远高于系统要求的装配公差极限，完成自由曲面离轴三反系统装配，近红外光波段全视场波像差RMS小于0.093λ，长波红外波段全视场波像差RMS小于0.126λ，中心视场波像差RMS为0.079λ。该方法具有良好的应用前景，将该方法应用于分离式结构装调，

在主镜三镜一体化结构中也有较高的应用价值，利用 CGH 高精度定位可以实现共基底加工误差的校准。该方法可广泛应用于自由曲面离轴系统装调、含自由曲面光学系统设计等领域。

## 参 考 文 献


[1] 孟庆宇 . 三镜反射式光学系统综述[J]. 红外与激光工程, 2022, 51(1): 20210986.
Meng Q Y. Overview of three-mirror reflective optical system [J]. Infrared and Laser Engineering, 2022, 51(1): 20210986.

[2] 王合龙, 陈建发, 黄浩阳, 等 . 基于自由曲面的离轴三反光学系统研制[J]. 红外与激光工程, 2023, 52(3): 20220523.
Wang H L, Chen J F, Huang H Y, et al. Development of off-axis three-mirror system based on free-form surface[J]. Infrared and Laser Engineering, 2023, 52(3): 20220523.

[3] 王超, 张新, 王灵杰, 等 . 离轴自由曲面三镜反射系统的装调技术[J]. 光学学报, 2013, 33(12): 1208001.
Wang C, Zhang X, Wang L J, et al. Adjustment of three-mirror off-axis freeform system[J]. Acta Optica Sinica, 2013, 33(12): 1208001.

[4] 王超, 张新, 王灵杰, 等 . 方形孔径自由曲面反射式系统装调技术研究[J]. 红外与激光工程, 2015, 44(5): 1518-1525.
Wang C, Zhang X, Wang L J, et al. Adjustment of abnormity aperture off-axis freeform system based on square aperture[J]. Infrared and Laser Engineering, 2015, 44(5): 1518-1525.

[5] 庞志海 . 离轴反射光学系统计算机辅助装调技术研究[D]. 西安: 中国科学院西安光学精密机械研究所, 2013.
Pang Z H. Research on computer aided alignment technology of off-axis reflective optical system[D]. Xi′an: Xi′an Institute of Optics and Precision Mechanics, Chinese Academy of Sciences, 2013.

[6] 李蕾 . 基于 Zernike 矢量多项式的离轴反射系统装调技术研究[D]. 长春: 中国科学院长春光学精密机械与物理研究所, 2020.
Li L. Research on adjustment technology of off-axis reflection system based on Zernike vector polynomial[D]. Changchun: Changchun Institute of Optics, Fine Mechanics and Physics, Chinese Academy of Sciences, 2020.

[7] 黎发志, 郑立功, 闫锋, 等 . 自由曲面的 CGH 光学检测方法与实验[J]. 红外与激光工程, 2012, 41(4): 1052-1056.
Li F Z, Zheng L G, Yan F, et al. Optical testing method and its experiment on freeform surface with computer-generated hologram[J]. Infrared and Laser Engineering, 2012, 41(4): 1052-1056.

[8] 姜晰文, 赵金宇, 吕天宇, 等 . 大口径主焦点式光学系统的设计与装调[J]. 光学 精密工程, 2022, 30(23): 2987-2994.
Jiang X W, Zhao J Y, Lü T Y, et al. Design and alignment of large-aperture prime focus optical system[J]. Optics and Precision Engineering, 2022, 30(23): 2987-2994.

[9] 李小燕, 付兴, 王鹏, 等 . 非球面光学反射镜的装调方法[J]. 应用光学, 2013, 34(3): 498-502.
Li X Y, Fu X, Wang P, et al. Alignment method of aspheric optical reflector[J]. Journal of Applied Optics, 2013, 34(3): 498-502.

[10] 陈太喜, 伍雁雄 . 航空机载紧凑型长焦距光学系统设计与装调[J]. 光子学报, 2021, 50(11): 1111002.
Chen T X, Wu Y X. Design and alignment of airborne compact long focal length optical system[J]. Acta Photonica Sinica, 2021, 50(11): 1111002.

[11] 周丽军, 杨通, 高丽娜, 等 . 易于多面共体加工的自由曲面离轴三反系统设计[J]. 光学学报, 2023, 43(8): 0822021.
Zhou L J, Yang T, Gao L N, et al. Design of freeform off-axis three-mirror system enabling multisurface-integrated fabrication [J]. Acta Optica Sinica, 2023, 43(8): 0822021.

[12] 朱德燕, 唐骏伟, 国成立, 等 . 计算全息板干涉检测工业镜头凸自由曲面[J]. 红外与激光工程, 2022, 51(9): 20220456.
Zhu D Y, Tang J W, Guo C L, et al. Interference detection of convex free-form surface of industrial lens by computer holographic plate[J]. Infrared and Laser Engineering, 2022, 51(9): 20220456.

[13] 张海涛, 徐乐, 谢常青 . 计算全息图案位置误差致波前误差的标定方法[J]. 光学学报, 2023, 43(8): 0822027.
Zhang H T, Xu L, Xie C Q. Calibration method of pattern place error-induced wavefront distortion with complex-phase computer-generated holograms[J]. Acta Optica Sinica, 2023, 43(8): 0822027.

[14] 孟庆宇 . 反射式光学系统误差敏感度理论及降敏设计方法研究[D]. 哈尔滨: 哈尔滨工业大学, 2021.
Meng Q Y. Research on error sensitivity theory and desensitization design method of reflective optical system[D]. Harbin: Harbin Institute of Technology, 2021.

[15] 曹宇泽, 马文礼 . 两步式灵敏度矩阵法在卡塞格林望远镜装调中的应用[J]. 光电工程, 2020, 47(2): 5-12.
Cao Y Z, Ma W L. Application of two step sensitivity matrix method in Cassegrain telescope alignment[J]. Opto-Electronic Engineering, 2020, 47(2): 5-12.

[16] 高松涛, 武东城, 于长淞 . 用于高精度非球面面形检测的计算全息图的设计[J]. 激光与光电子学进展, 2016, 53(9): 090901.
Gao S T, Wu D C, Yu C S. Computer-generated hologram design for high-precision aspherical surface testing[J]. Laser & Optoelectronics Progress, 2016, 53(9): 090901.

[17] 杨增鹏, 李政言, 浦恩昌, 等 . 基于离轴三反光学系统的高分辨率中阶梯光栅光谱仪[J]. 光学学报, 2021, 41(22): 2212001.
Yang Z P, Li Z Y, Pu E C, et al. High-resolution echelle grating spectrometer based on off-axis three-mirror reflective optical system[J]. Acta Optica Sinica, 2021, 41(22): 2212001.

# Alignment Method for Off-Axis Optical Systems Based on CGH Multi-Mirror Attitude Determination

Wu Yifan[1,2], Chen Jianfa[1,2*], Cui Zeyao[1,2], Huang Haoyang[1,2]

[1]*Luoyang Institute of Electro-Optical Equipment, Aviation Industry Corporation of China, Ltd., Luoyang* 471009, *Henan, China*;

[2]*National Key Laboratory of Space Based Information Perception and Fusion, Luoyang* 471009, *Henan, China*

## Abstract

**Objective** The development trend of onboard electro-optical systems towards multifunctionality, high performance, and light weight poses higher demands on the development of optical systems. Reflective optical systems are widely employed in various types of onboard electro-optical devices due to their broad bandwidth and compact working characteristics, and they face challenges such as obscuration of secondary mirrors, limited field of view, and low optimization degrees in traditional coaxial reflective systems. Off-axis three-mirror reflective optical systems with freeform surfaces can address these issues. However, the development and maturity of freeform surface design and manufacturing techniques pose challenges to freeform surface shape measurement and system alignment. In previous studies, computer-generated holograms (CGHs) are adopted for single mirror shape measurement, but there is limited publicly available information on multi-mirror shape measurement with CGHs and their joint baseline design.

**Methods** We propose a method for CGH joint baseline design of multi-mirror shape measurement to enable independent high-precision positioning of each mirror during alignment. The core idea is to combine detection and design to ensure high-precision shape measurement and achieve high-precision positioning and stabilization of multiple mirrors. The specific process of the joint baseline design for multi-mirror CGHs is as follows (Fig. 1). 1) The input parameters for the mirror shape are set, including posture parameters and surface parameters. 2) The initial point for CGH posture optimization is calculated based on the parameters. Additionally, CGH posture parameters (tilt and distance from the measured surface) are optimized to ensure the integrity and moderate size of the holographic areas for primary mirror and third mirror. 3) Additional holographic areas are designed based on posture parameters, including rough alignment areas, angular alignment areas, and interference order marking areas. The angular alignment area utilizes a reflective grating design with the shining angle set as the incident angle of the interferometer′s light rays. 4) The manufacturability of the designed fringe patterns is examined. If the patterns meet the processing requirements, the joint baseline design is considered complete to proceed to system alignment. Otherwise, the first step should be returned and the design parameters should be readjusted until the fringe patterns meet the processing requirements. The alignment process using multi-mirror joint baseline design CGH is as follows (Fig. 3). 1) The two-mirror posture optimization CGH design is finished based on the system parameters. 2) The CGH alignment baseline is set, the interferometer is aligned with the main mirror alignment area, and the alignment of the interferometer and the main mirror is fixed. 3) The primary mirror is aligned. The interferometer posture is adjusted based on the alignment area of the main mirror interferometer. The misalignment is reflected by the sensitivity matrix of the detection optical path. According to the sensitivity matrix theory, under small misalignment, Zernike polynomial coefficients are linearly related to the misalignment. The main mirror should be fine-tuned based on interferometric fringe Zernike coefficients. 4) The third mirror is aligned. The interferometer posture is adjusted based on the alignment area of the three-mirror interferometer and the third mirror are fine-tuned based on the interferometric fringe Zernike coefficients. Meanwhile, the posture and stabilization of primary mirror and third mirror are completed. 5) The system alignment baseline is established by the interferometer, and a theodolite is employed to align the system baseline and the reticle at the exit pupil. 6) The secondary mirror is aligned. A collimated laser is adopted to position the tilt and pitch of the secondary mirror. 7) The secondary mirror is fine-tuned to achieve the desired image quality at the zero field of view. 8) The angles of the interferometer and the collimated mirror are adjusted to the off-axis field of view, and the imaging quality at the off-axis field of view is measured. If it meets the design requirements, system alignment is ended. Otherwise, the zero field of view should be returned and the wavefront error adjustment should be continued until the off-axis field of view also meets the design requirements.

**Results and Discussions** The CGH design is limited by the following factors, including minimum stripe width greater than 1.5 μm, single holographic area diameter smaller than 80 mm, and complete CGH diameter smaller than 160 mm. The designed CGH (Fig. 5) with minimum stripe width 1.78 μm meets the manufacturing process and design requirements. The fabrication error analysis can simplify the model to a linear grating model (Fig. 7). The main fabrication errors (Table 2) contain substrate shape error, stripe width error, etching depth error, and stripe duty cycle error. Among them, the substrate shape error has the most significant influence on CGH imaging. However, the substrate′s manufacturing accuracy is smaller than $\lambda/100$ and does not affect subsequent preparation of etched stripes. The other errors cause wavefront error changes within the tolerance range and have a minimal effect on CGH positioning accuracy. In production, it is essential to first suppress substrate shape errors and then pay attention to stripe width errors, further improving the precision of CGH shape measurement. Transmission wavefront measurement (Fig. 8) is performed on the fabricated CGH product. The comprehensive wavefront error in the measured CGH is less than $\lambda/80$, which meets the requirements for shape measurement accuracy. In the experiment (Table 3), the main mirror is aligned first, and the RMS of the single mirror shape is $0.022\lambda$. Then, the three mirrors are aligned and the RMS of the single mirror shape is $0.032\lambda$, which satisfies the design requirement that the RMS of the single mirror alignment shape should be less than $0.050\lambda$. Finally, the secondary mirror is aligned. In the full-field imaging quality test (Table 6), the field angle adjustment is realized via theodolite positioning and optical system rotation. The RMS wavefront aberration in the near-infrared wavelength range is less than $0.093\lambda$, and in the long-wave infrared wavelength range, it is less than $0.126\lambda$. The RMS wavefront aberration at the central field of view is $0.079\lambda$, which meets the design requirements for imaging quality.

**Conclusions** This method has excellent application prospects. Meanwhile, it is applied to separate structure alignment in this study and has application significance in the off-axis three-mirror integrated structures. High-precision positioning using CGH can calibrate the common baseline machining errors. This method can be widely adopted in the alignment of freeform off-axis systems and the design of optical systems with freeform surfaces.

**Key words** optical design; computer-generated hologram; off-axis three-mirror; freeform surface